Journal of Applied Polymer Science

Separation of oil/water emulsions using nano MgO anchored hybrid ultrafiltration membranes for environmental abatement

Thanigaivelan Arumugham,[1] Noel Jacob Kaleekkal,[1] Dipak Rana,[2] Mohan Doraiswamy[1]

[1]Membrane Laboratory, Department of Chemical Engineering, Anna University, Chennai 600025, India

[2]Department of Chemical and Biological Engineering, Industrial Membrane Research Institute, University of Ottawa, 161 Louis Pasteur St., Ottawa, Ontario, Canada K1N 6N5

Correspondence to: D. Mohan (E-mail: mohantarun@gmail.com)

ABSTRACT: This work focuses on utilizing the dual role of sulfonated polyphenyl sulfone (SPPSU) as both an anchoring agent and an interlayer modifying agent in the preparation of nano MgO/SPPSU/PPSU membranes for oil removal from water. These asymmetric membranes were prepared using the phase inversion technique. The dispersed nano MgO was observed in the membrane matrix as seen by scanning electron microscope and energy dispersive X-ray analysis. The reduction in contact angle value establishes the increases in hydrophilicity. An increase in SPPSU (wt %) loosens the nano MgO/SPPSU/PPSU membrane packing as exhibited by the increase of *d*-spacing by X-ray diffraction analysis. The antifouling properties were tested using humic acid, as a model foulant. Further, in castor oil/water emulsion separation, it was found that the membrane with 25 wt % anchored moiety SPPSU/nano MgO produced a greater flux recovery ratio of 94.9% (±0.3) without compromising the oil rejection of 99% (±0.4) and better oleophobic surfaces for oil. © 2015 Wiley Periodicals, Inc. J. Appl. Polym. Sci. **2016**, *133*, 42848.

KEYWORDS: hydrophilic polymers; membranes; morphology; self-assembly; separation techniques

Received 23 June 2015; accepted 17 August 2015

DOI: 10.1002/app.42848

INTRODUCTION

A large quantity of oily wastewater is discharged regularly from various chemical, metallurgical, pharmaceutical, and food industries.[1] The rapid growth and expansion of these industries result in an increasing of carbon content in fresh water resources. The oil in water can be classified as a free floating oil (>150 μm), unstable dispersed oil (20–150 μm) and stable emulsion (<20 μm).[2] Of these, the stable emulsion droplet cannot be removed effectively using conventional methods like floating, chemical coagulation, and thermal treatment.[3] Membrane technology offers a promising solution for the removal of stable oil/water emulsion (O/W). Microfiltration and ultrafiltration membrane processes are more widely used than nanofiltration for oil–water filtration. To maintain the better permeate quality, ultrafiltration is more suitable than microfiltration (MF). Moreover, most of the membrane companies recommend the membrane cutoff in the range of 20-50 kDa for oil/water emulsion removal.[4,5]

PPSU is a material of great interest in fabricating ultrafiltration (UF) membranes. This is because the phenylsulfone moiety provides excellent physiochemical properties, such as molecular stiffness, amorphous nature, wriggle resistance, thermal stability (T_g 208°C) and dimensional stability.[6] However, the inherent hydrophobic nature of PPSU membranes restricts its application in liquid phase applications. This is mostly due to the nonspecific interaction of foulants with the surface and pores of the membranes, which is termed as membrane fouling. In fact, fouling mainly depends on the physiochemical properties of membrane surface, feed solution chemistry, and nature of foulants. Reversible fouling is due to the weak interaction of foulants with the membrane surface and can be cleaned by simple back washing. Foulants that are plugged strongly into the membrane pores contribute to the irreversible fouling.

Even chemical cleaning processes cannot completely remove the irreversibly plugged foulants.[7] Moreover, operation cost, energy demand, membrane lifetime and performance are severely suppressed by these chemical cleaning agents.[8] Hence, the preparation of self cleaning membranes can be an effective way to improve the antifouling property of the membranes. Increasing hydrophilicity of the membrane surface strongly reduces the attachment of foulants.[9] Various modification techniques, such as coating, blending, composite, grafting, bulk modification, etc. are being used to improve membrane hydrophilicity.[10] Introduction of nano particles are currently receiving wide attention in membrane research. Nanoparticles, such as ZnO,[11] Al_2O_3,[12] carbon nanotubes,[13] graphene oxide,[14] Cu,[15] and Ag[16] have

incorporated to increase of antifouling properties of membranes. Nano magnesium oxide (MgO) is an excellent nanomaterial with superior characteristics, such as high hydrophilicity, high surface area, nontoxicity for human beings, antibacterial activity, environment friendly, low cost, high mechanical strength, and thermal stability.[17,18] The toxicity of the various nano particles such as Ag, TiO_2, CNT, ZnO, MgO were assessed by Wei et al. for nano reienforced food package application.[19] They reported that when compared with Ag NPs, ZnO, and other nanoparticles, the MgO NPs proved to be safer, and also has a greater ability to inhibit the growth of microorganisms.

Very few reports are mentioned in literature about MgO incorporated ultrafiltration membranes. It could be because of its nonuniform dispersion within hydrophobic polymer matrix.[20] Ahmad *et al.* pointed out that incorporation of hydrophilic polyelectrolyte chains can provide a better dispersion for nanoparticles.[5,21] So, this work was performed to deal with the preparation and characterization of nano MgO composite membranes to improve the surface property of PPSU based ultrafiltration membranes. Further, to solve the limitation of non uniform dispersion of the NPs, we have fabricated surface localized nanocomposite membranes based on the electrostatic interaction between nanoaparticles and polymeric chains.[22]

In this work, nano MgO/SPPSU/PPSU composite membranes were fabricated as new self cleaning membrane material. Here, various concentrations of polyelectrolyte chains SPPSU were used to anchor the nanoparticles and aid their dispersion within the PPSU membrane matrix. The nonsolvent induced phase separation method was used to prepare the nano MgO/SPPSU/PPSU composite membranes with the addition of SPPSU (0, 5, 10, 15, and 25 wt %). These nanocomposite membranes were studied in detail using energy dispersive X-ray spectroscopy (EDX), scanning electron microscope (SEM), X-ray diffraction (XRD), contact angle (CA), porosity, mean pore size, molecular weight cutoff (MWCO), and pure water flux (PWF). The prepared membranes were used to filter model foulants such as humic acid (natural organic matter) and castor oil/water emulsion in a dead-end ultrafiltration kit. The antifouling properties of membranes were investigated in terms of reversible fouling analysis (R_r, %), irreversible fouling analysis (R_{ir}, %), flux recovery ratio (FRR, %), and resistances were calculated by assuming in a series model.

MATERIALS AND METHODS

Polyphenylsulfone (PPSU, M_w: 53–59 kDa) was used as a base polymer for membrane preparation after drying at 80°C for 12 h, Chlorosulfonic acid (99%), Sodium azide (≥9.5%), magnesium nitrate hexahydrate, Bioxtra ≥98%, as a starting material for synthesis of magnesium oxide (MgO) nanoparticles, were received from Sigma-Aldrich. Calcium chloride, *N*-methyl-2-pyrolidone, extra pure (NMP, from Sisco Research), ammonia solution 25% (GR), polyethylene glycol (PEG M_w: 600 Da) was received from Merk Specialties, India. Sodium laryl sulphate (SLS, pure), (Sisco Research). Molecular Sieve 3Å (purified), humic acid, dextran (M_w: 40, 70 kDa) from HiMedia Laboratories. Commercial castor oil, ethyl alcohol (AR), 99% v/v min was received from Hayman Speciality Products. Pure distilled water was used to prepare the coagulation bath.

Synthesis of MgO Nanoparticles

The synthesis of MgO nanoparticles was carried out based on previous reported literature with slight modification.[23] All of the chemicals were taken with an analytical grade and were used for the reaction without further purification. At first, 0.1 wt % PEG 600 was dissolved in 50 mL of 0.1*M* $Mg(NO_3)_2$ solutions in the round bottom flask, stirred for 15 min to make a homogeneous solution using a magnetic stirrer. After that the pH was maintained at 10 by adding ammonium hydroxide in a dropwise manner. Then, the reaction mixtures were stirred for 1.5 h at 50°C. The resulting magnesium hydroxide was formed as a white precipitate. The resultant precipitate was collected by using centrifugation, washed several times with distilled water and ethanol to remove unwanted impurities. The resulting white magnesium hydroxide precipitate was dried in hot air from an oven at 80°C and calcination was carried out at 450°C for 2 h to produce the white nano magnesium oxide powder. The dried nano MgO powder formed was characterized using X-ray diffraction (Bruker AXS D8 Advance X-ray diffractometer) and transmission electron microscope (JEOL JEM-2010F).

Synthesis of Sulfonated Polyphenylsulfone (SPPSU)

The detailed information about the synthesis and characterization of the sulfonation on polyphenylsulfone (SPPSU) was given in our previous research work.[24]

Membrane Preparation Technique

Varying the percentage of SPPSU (different wt %) was used to fabricate the nano MgO anchored hybrid polyphenylsulfone ultrafiltration membranes using the phase inversion technique[25] (see Figure 1). The composition of casting solution for all membranes are listed in Table I. Initially, magnesium oxide nanoparticles (0.25 wt %) were dispersed in the NMP solvent and ultrasonicated for 30 min. After sonication, the SPPSU and PPSU were dissolved in the dope solution by stirring for 12 h to get a homogeneous polymer casting solution. After that the viscous polymeric casting solution was kept for 4 h to remove air bubbles. Then, homogeneous casting solutions were cast uniformly on the polished glass plate using Doctor's blade under a controlled environment such as relative humidity (25 ± 2%), temperature (40°C) to avoid fast precipitation in the casting solution due to atmospheric moisture. Meanwhile, the coagulation bath was prepared with particular compositions, such as 2% v/v of NMP (solvent), 0.2 wt % of SLS (surfactant) in 2 L of distilled water at 14 ± 2°C.

Subsequently, the glass plate was immersed into the coagulation bath to initiate the phase inversion process. The resultant membranes were peeled off, washed with distilled water to remove residual solvents and surfactant then stored in distilled water containing sodium azide (100 mg/L) to avoid unwanted bacterial growth on the surface of the membranes. All the membranes were prepared with uniform thickness (0.22 ± 0.02 mm) and checked using a digimatic caliber with a precision of 0.001 mm.

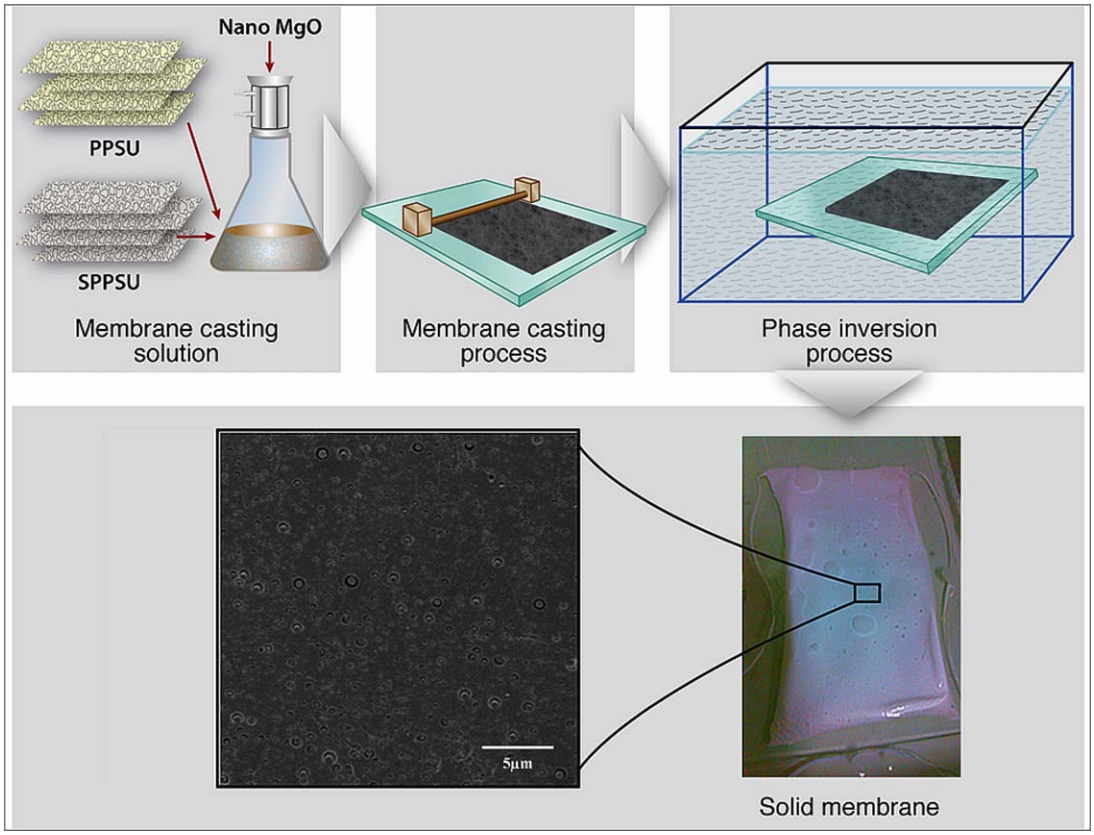

Figure 1. Asymmetric membrane preparation scheme. [Color figure can be viewed in the online issue, which is available at wileyonlinelibrary.com.]

CHARACTERIZATION OF MEMBRANES

Analysis of Membrane Morphology

The prepared membranes were characterized using scanning electron microscope (SEM, Cam Scan MV 2300). The small piece of membranes was cut and freeze-dried in liquid nitrogen for 60–90 s. Before SEM analysis, the nonconducting membranes were gold sputtered to make electrical conductivity on the membrane surface, cross section, and surface images were then captured under high vacuum (10 kV) condition.

Energy Dispersive X-ray Spectroscopy (EDX)

The membranes were cut into desired shape to identify the elements present on the surface of membranes using Oxford Instrument nanoanalysis INCA energy 250 microanalysis system (EDX) under higher vacuum at 10 kV. Each sample was analyzed at three different locations and reported.

Table I. Composition of the Membranes

Membrane	PPSU (wt %)	SPPSU (wt %)	Nano MgO (wt %)	NMP (wt %)
a1	100	-	-	84
a2	100	-	0.25	83.7
a3	95	05	0.25	83.7
a4	90	10	0.25	83.7
a5	85	15	0.25	83.7
a6	75	25	0.25	83.7

Note: total polymer concentration at 16 wt %.

Contact Angle of the Membranes

The prepared membranes were cut into (2 cm × 2 cm) size, washed completely in distilled water, and the surface of the membrane mobbed with tissue paper. Then, contact angles of all membranes were measured using GBX instrument, Germany at 25°C.[26] Volume of 2 μL of milli-Q water was placed on the membrane to form a sessile drop, angle of the sessile drop was measured within 10 s, at five different locations for each membrane and an average value of the angle was reported.

Pure Water Flux (PWF)

Before the experiment, all membranes were compacted at 414 kPa. Then, the pure water permeation was measured for all prepared membranes for every one hour in the UF cell (Model 8400, Amicon) with an internal diameter of 76 mm at a specific operating pressure (345 kPa) at 25°C. The amount of pure water flux (Jw_1) was calculated using eq. (1). For each membrane, the pure water flux experiment (Jw_1) was conducted in three different areas and average values were reported for accuracy.

$$Jw_1 = \frac{Q}{A(\Delta t)} \quad (1)$$

Q is the quantity of permeate (in litre, L); A is the effective membrane area (m^2); Δt is the time (h)

Analysis of Porosity and Mean Pore Size (Nm) of the Membranes

The gravimetric method was used to calculate the porosity (ε, %) of all prepared membranes.[27] This can be defined as the ratio between the amount of water content present in the pores and total membrane volume.

The given eq. (2) was used to determine the porosity of the membranes and the average value of five experiments were reported for each membrane,

$$\varepsilon(\%) = \frac{W_0 - W1}{\rho A h} \times 100 \quad (2)$$

where W_0 is the wet weight of the membrane; W_1 is the dry weight of the membrane; ρ is the density of water (0.998 g cm^{-3}); A is the effective membrane area (m^2); h is the membrane thickness (cm).

Guerout–Elford–Ferry eq. (3) was used to calculate the mean pore size (r_m) of all prepared membranes based on the results of pure water flux (Jw1) and porosity value.

$$r_m = \sqrt{\frac{(2.9 - 1.75\varepsilon)8\eta h Q}{\varepsilon \times A \times \Delta P}} \quad (3)$$

where η is the water viscosity (8.9×10^{-4} Pa s), Q is the quantity of permeate per unit time (m^3 S^{-1}), ΔP is the operating pressure (345 kPa), h is the membrane thickness (m) and ε is the porosity of the membranes.

X-ray Diffraction (XRD) Analysis

The membranes were characterized using wide angle X-ray diffraction pattern (Bruker AXS D8 Advance X-ray diffractometer).[28] The diffraction patterns were recorded within the range of 5°–10° using CuKα radiation ($\lambda = 1.54$ Å).

Molecular Weight Cutoff (MWCO) Analysis

The experiment was performed with UF cell (Model 8400, Amicon), dead end filtration setup at 345 kPa using 0.2 g/L of dextran (40 and 70 kDa) solution to determine the pore size of the membranes.[29] Total organic carbon analyzer (Shimadzu, TOC-V CPH) was used to analyze the concentration of feed and permeate of the corresponding membranes.

The rejection of membranes was calculated using the formula given below,[30]

$$SR(\%) = \left[1 - \frac{C_p}{C_f}\right] \times 100 \quad (4)$$

C_p is the concentration of permeate (g/L); C_f is the concentration of feed (g/L).

Analysis of Permeation and Rejection Properties of Membranes

All prepared membranes were tested with a pure water permeation rate at 345 kPa for 5 h. Model foulant, the humic acid feed solution was prepared by dissolving 0.3 g of a humic acid substance in 1L of pure distilled water containing 0.01M $CaCl_2$, pH = 8. All membranes were operated at constant pressure of 345 kPa for 3 h in the dead end ultrafilter cell. Here, concentration polarization infiltration was minimized effectively by stirring at 500 rpm. Similarly, 1 mg/mL of castor oil/water emulsion was prepared by stirring at 1000 rpm for 5 h. The average size of the oil emulsion droplets was 1.46 μm, which was measured using the Malvern Instruments particle size analyzer (Zetasizer ver.6.20, MAL 1049897). A fresh set of membranes were taken for each feed solution. The rate of permeation was calculated using following eq. (5) at different time interval,

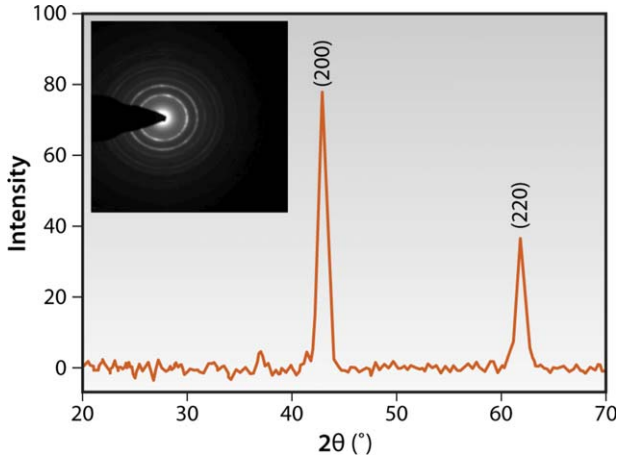

Figure 2. X-ray diffraction spectroscopy (XRD) of magnesium oxide (MgO) nanoparticles. [Color figure can be viewed in the online issue, which is available at wileyonlinelibrary.com.]

$$J_{(h,O)} = \frac{Q}{A(\Delta t)} \quad (5)$$

J_h is the flux of humic acid solution (Lm^{-2} h^{-1}), J_o is the flux of oil/water emulsion acid solution (Lm^{-2} h^{-1}), Q is the quantity of permeate (in litre, L) (L), A is the area of membrane (m^2), and Δt is the permeate time (h).

To evaluate the membrane rejection performance, the collected permeate and feed solution of humic acid and oil/water emulsion was analyzed using the total organic carbon analyzer (Shimadzu, TOC-V CPH). The rejection percentage of membranes were calculated based on the carbon content in the sample using eq. (4). After that the membrane surfaces were cleaned using pure distilled water for humic acid (HA) fouled membranes and 0.5% SLS for oil fouled membranes for 20 min. Again the pure water flux experiment was carried out for those membranes.

Fouling Evaluation by Using Resistance-in-Series Model

The membrane resistance properties were analyzed in depth by using resistance in series model. Here, the extent of membrane resistance against the flow of the water molecule, humic acid solution, and oil/water emulsion was analyzed during the filtration process across the membrane surface. The following equations[31] were used to determine the membrane resistance against the flow.

$$J = \frac{\Delta P}{\mu R t} \quad (6)$$

$$R_t = R_m + R_c + R_p \quad (7)$$

where R_m is the hydraulic resistance (m^{-1}), R_c is the resistance due to the cake layer formed on the membrane surface (m^{-1}), R_p is the resistance due to the solute plugging into the pore wall during filtration (m^{-1}).

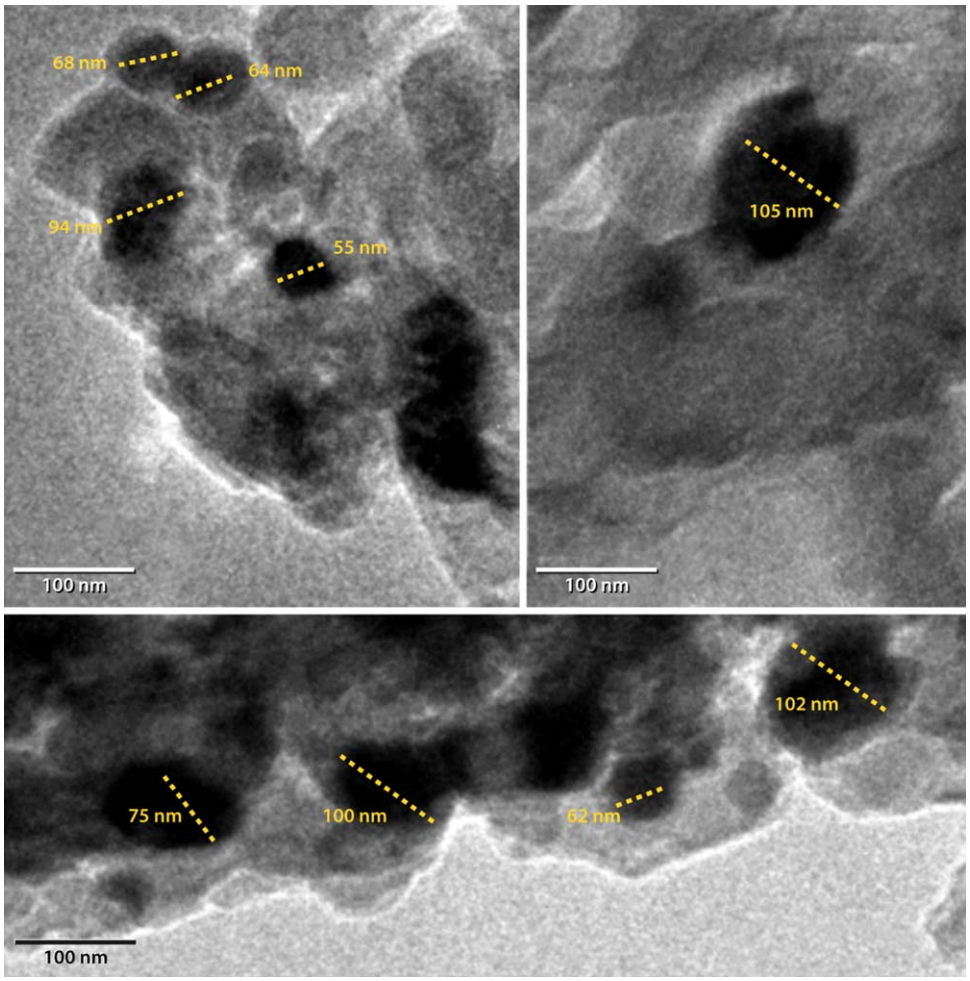

Figure 3. Transmission electron microscope (TEM) analysis of magnesium oxide (MgO) nanoparticles. [Color figure can be viewed in the online issue, which is available at wileyonlinelibrary.com.]

Each resistance can be calculated using the following equations:

$$R_m = \frac{\Delta P}{\mu J_{w1}} \tag{8}$$

$$R_p + R_c = \frac{\Delta P}{\mu J_{(h,o)}} - R_m \tag{9}$$

$$R_p = \frac{\Delta P}{\mu J_{w(2,3)}} - R_m \tag{10}$$

where, J_{w1} is the pure water flux of the membranes, J_h is the flux of humic acid solution ($Lm^{-2}\ h^{-1}$), J_o is the flux of oil/water emulsion acid solution ($Lm^{-2}\ h^{-1}$), J_{w2} is the pure water flux after humic acid filtration ($Lm^{-2}\ h^{-1}$); J_{w3} is the pure water flux after castor oil/water emulsion filtration ($Lm^{-2}\ h^{-1}$), ΔP is the operating pressure during membrane filtration, μm is the viscosity of the permeate solution.

Analysis of Membrane Fouling and Reusability

The membrane surface fouling was evaluated in terms of reversible and irreversible membrane pore plugging using eqs. (11)

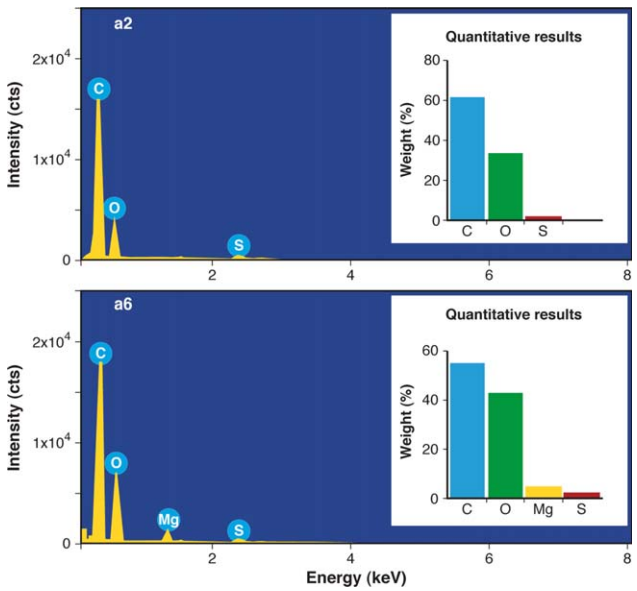

Figure 4. Energy dispersive X-ray spectroscopy (EDX) images of membranes. [Color figure can be viewed in the online issue, which is available at wileyonlinelibrary.com.]

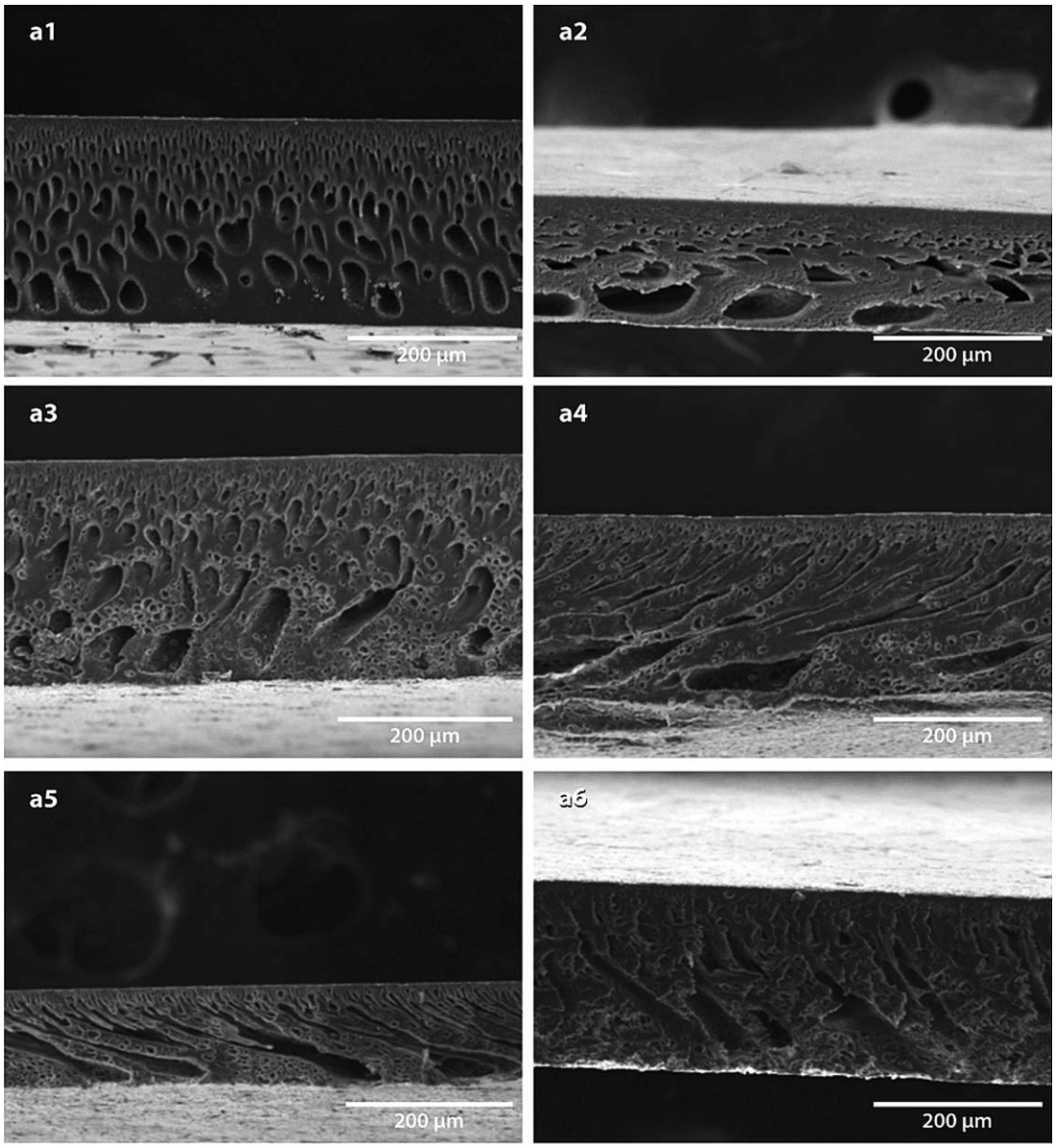

Figure 5. Cross-sectional images of pure and modified PPSU membranes.

and (12). Further, the reusability of membranes were analyzed after cleaning and calculated using eq. (13).[32]

Reversible Fouling

$$R_r = \frac{J_{w(2,3)} - J_{w(h,o)}}{J_{w1}} \times 100 \quad (11)$$

Irreversible Fouling

$$R_{ir} = \frac{J_{w1} - J_{w(2,3)}}{J_{w1}} \times 100 \quad (12)$$

Flux recovery ratio

$$FRR(\%) = \frac{J_{w(2,3)}}{J_{w1}} \times 100 \quad (13)$$

J_{w1} is the pure water flux ($Lm^2\ h^{-1}$): J_h is the flux of humic acid solution ($Lm^{-2}\ h^{-1}$), J_o is the flux of oil/water emulsion acid solution ($Lm^{-2}\ h^{-1}$), J_{w2} is the pure water flux after humic acid filtration ($Lm^{-2}\ h^{-1}$); J_{w3} is the pure water flux after castor oil/water emulsion filtration ($Lm^{-2}\ h^{-1}$).

RESULTS AND DISCUSSION

Characterization of Nano MgO Particles

The characteristic XRD peaks of nano MgO are shown in Figure 2. The diffracted peaks were indexed using JCPDS (78-0430). The 2θ peaks at 42.6° and 61.7° correspond to (200) and (220) planes, respectively.[33] The TEM image of nano MgO particles is as shown in Figure 3. Further, the size distribution of the distorted nano cube was measured using ImageJ software. It is observed to be in the range of 55–105 nm. All these results via XRD and TEM collectively confirmed the formation of nano MgO particles.

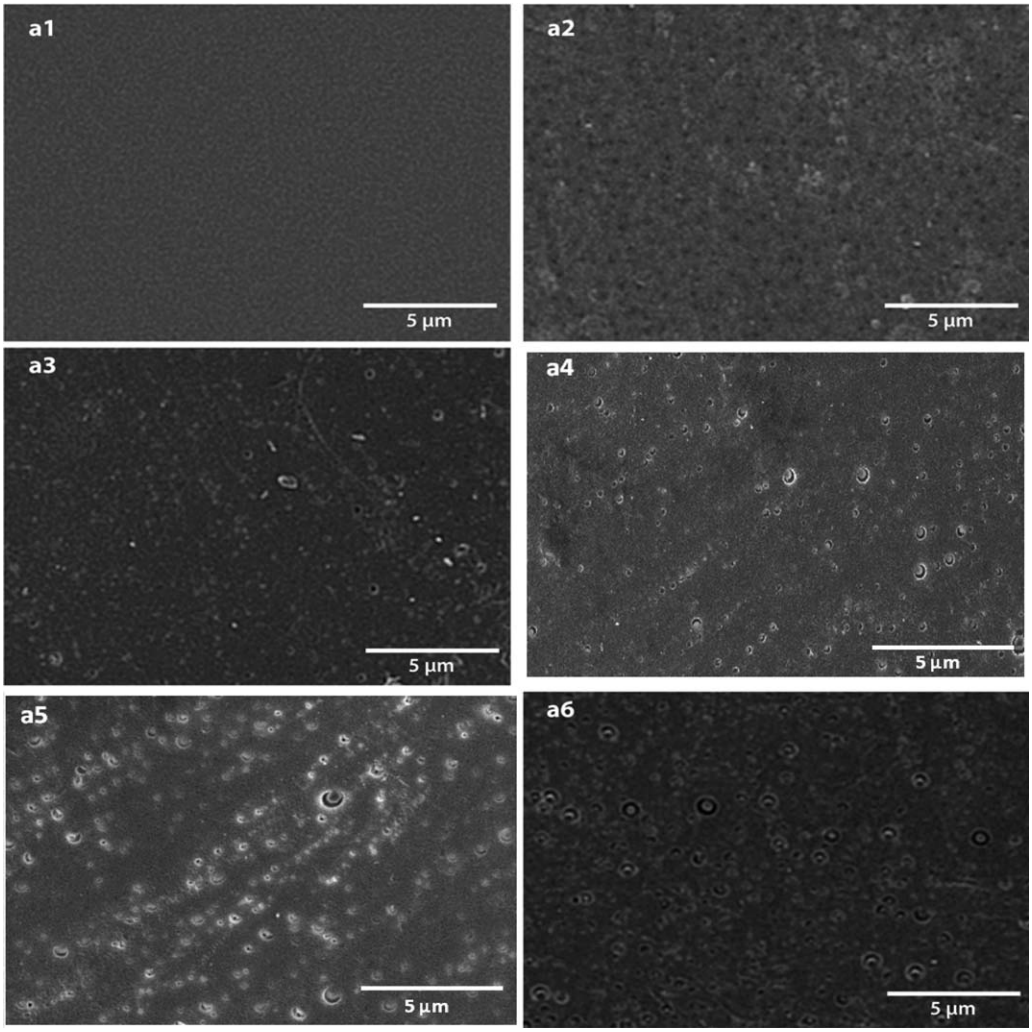

Figure 6. Top surface images of pure and modified PPSU membranes.

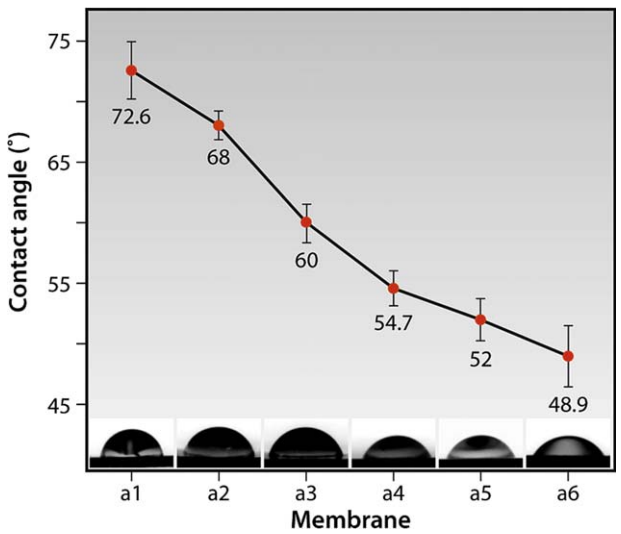

Figure 7. Contact angle results of the pure and modified PPSU membranes. [Color figure can be viewed in the online issue, which is available at wileyonlinelibrary.com.]

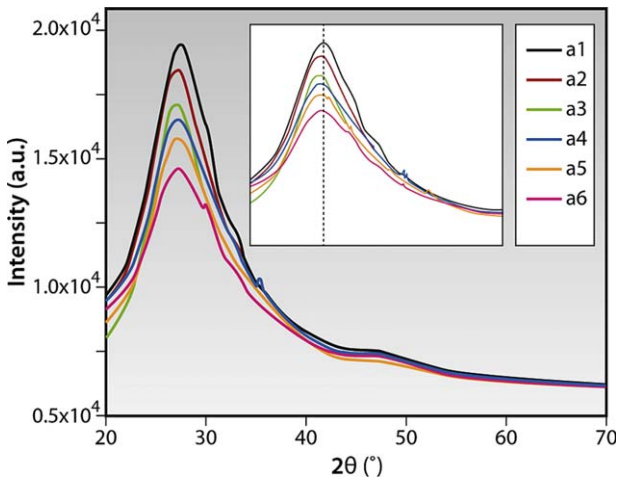

Figure 8. X-ray diffraction (XRD) pattern of pure and modified PPSU membranes. [Color figure can be viewed in the online issue, which is available at wileyonlinelibrary.com.]

Table II. Porosity, MWCO, Mean Pore Size, and d-Spacing of the Membranes

Membrane	Porosity (%)	MWCO (kDa)	Mean pore size (nm)	*d*-spacing (nm)
a1	24.6 (±0.31)	40	15 (±0.21)	0.473 (±0.001)
a2	34.5 (±0.89)	40	15 (±0.29)	0.475 (±0.002)
a3	56.2 (±1.17)	40	21 (±0.23)	0.482 (±0.001)
a4	60.6 (±2.02)	40	23 (±0.40)	0.483 (±0.001)
a5	62.8 (±3.03)	40	23 (±0.57)	0.485 (±0.001)
a6	65.7 (±3.57)	70	24 (±0.76)	0.488 (±0.003)

Analysis of the Membrane Morphology

The EDX spectra was used to determine the surface chemical composition of the membranes (shown in Figure 4). The peak of the elemental magnesium (Mg) was observed for membrane a6, but not membrane a2. Concentration of Mg and O increased as seen from the EDX spectra which confirmed that the MgO nanoparticles are bound to the SPPSU polymeric chains and distributed uniformly on the membrane surfaces.

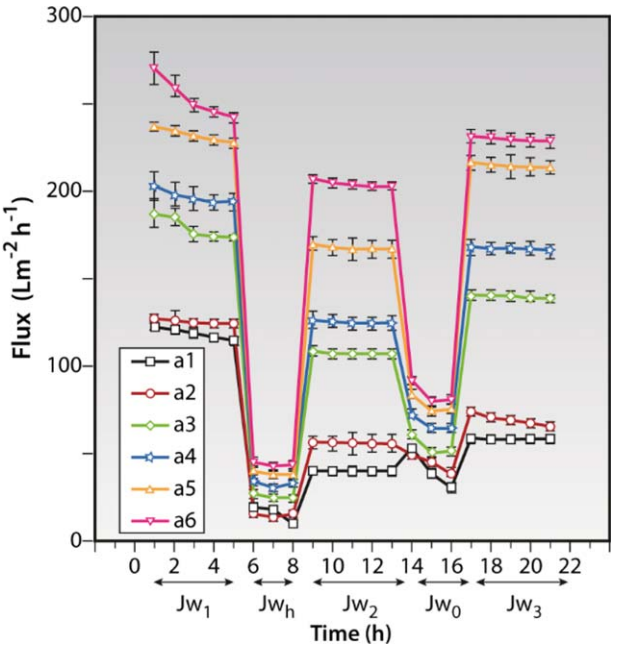

Figure 9. Intergrated flux profile of the pure and modified membranes. [Color figure can be viewed in the online issue, which is available at wileyonlinelibrary.com.]

Similarly, other researchers also established the incorporation of zinc oxide and silver loaded zirconium phosphate (AgZ) nanoparticles into the membrane matrix using EDX analysis.[34] Hence, we could affirm the vital role of sulfonic acid moiety in fixing the MgO nanoparticles on the SPPSU/PPSU membrane surfaces from the EDX results.

Figures 5 and 6 show the cross sectional and top surface morphologies of all membranes. The SEM image of membrane a2 shows a rigid PPSU membrane structure (Figures 5, 6, and a2). This is due to the strong interaction of nano MgO with solvent (NMP) which leads to an increase in viscosity of the casting solution. In an earlier work, it was[35] hypothesized that the membrane pore growth is regulated and restricted by the viscosity of the polymer casting solution. A high viscous solution decreases the mobility of polymeric chains and results in a poor solvent–nonsolvent exchange rate. However, the presence of MgO nanoparticles could not be seen on the membrane a2 surface. The EDX results are also in agreement with the morphological observation.

In the Figures 5 and 6 (a3–a6), drastic changes in the membrane morphology are noticed. On adding SPPSU, there arises an incompatibility in the interaction between the polymeric chains which had increases in the segmental volume gap. The increasing segmental volume permits more water molecules to penetrate which in turn forms pore nuclei. Further, the longer penetration of water molecules into the casted membranes improves the pore growth, which results in a higher interconnectivity between the top and bottom membrane surfaces.[36] Moreover, the presence of void volume facilitates the nano MgO particles migration towards the membrane top layer. The presence of hydrophilic SPPSU lowers the interfacial surface energy at the membrane–water interface and firmly anchors the

Table III. Flux, HA Rejection, and Fouling Analysis

Membrane	Flux (Lm^{-2} h^{-1})			R_r (%)	R_{IR} (%)	FRR (%)	Rejection (%) HA
	J_{w1}	J_h	J_{w2}				
a1	116 (±1.15)	20 (±1.08)	46.6 (±0.76)	22 (±0.28)	59.8 (±0.65)	40.2 (±1.2)	91.2 (±1.2)
a2	125 (±2.2)	23 (±0.07)	61.5 (±0.92)	30.7 (±0.74)	50.4 (±0.74)	49.2 (±0.6)	91.7 (±1.3)
a3	170 (±1.52)	32.7 (±1.54)	111 (±3.62)	44.9 (±1.86)	34.5 (±0.67)	65.4 (±0.57)	89.9 (±0.3)
a4	189 (±4.93)	39.8 (±1.88)	133 (±2.53)	48.9 (±1.52)	29.7 (±2.62)	70.2 (±0.72)	89.2 (±0.2)
a5	221 (±2.01)	45.4 (±1.93)	177 (±4.76)	59.2 (±0.65)	19.5 (±0.95)	80.4 (±1.32)	89.1 (±1.3)
a6	234 (±1.53)	49.7 (±2.65)	199 (±3.65)	63.5 (±0.93)	14.4 (±1.88)	85.5 (±1.14)	63.1 (±1.5)

Table IV. Results of Fouling Resistance in Series Model of Membranes for HA Substances

Membrane	Membrane resistance $R_m \times 10^{11}$ (m^{-1})	Pore plugging resistance $R_p \times 10^{11}$ (m^{-1})	Cake layer resistance $R_c \times 10^{11}$ (m^{-1})	Total resistance $R_t \times 10^{11}$ (m^{-1})
a1	1.20 (±0.01)	1.78 (±0.04)	3.96 (±0.36)	6.94 (±0.36)
a2	1.12 (±0.01)	1.16 (±0.03)	3.77 (±0.03)	6.05 (±0.01)
a3	0.82 (±0.21)	0.43 (±0.08)	3.06 (±0.21)	4.75 (±0.69)
a4	0.73 (±0.15)	0.31 (±0.18)	2.49 (±0.15)	3.91 (±0.72)
a5	0.63 (±0.07)	0.15 (±0.02)	2.27 (±0.36)	3.28 (±0.50)
a6	0.59 (±0.09)	0.11 (±0.07)	2.12 (±0.21)	3.03 (±0.21)

nano MgO particles on the surface.[37] These morphological analysis results prove that addition of SPPSU forms a loosely membrane-composite structure, and anchors the nano MgO particles on the membrane surfaces thereby altering the membrane surface properties.

Hydrophilicity of the Membranes

The contact angle values of all the prepared membranes are shown in Figure 7. Membrane hydrophilicity mainly depends on their surface chemical composition and generally, a hydrophilic surface has a lower contact angle value. The bare membrane exhibits highest hydrophobicity and showed a CA of 72° (±2.3); the CA value reduced to 48.9° (±2.1) for nano MgO anchored membranes. The reactive nano MgO is readily available on the membrane surface which has more surface hydroxyl group (—OH) and forms a stable hydration layer in water.[38] Hence, the uniform distribution of nano MgO within the SPPSU/PPSU matrix provides the polar membrane surface, which could form an aggregated water cluster via hydrogen bond interaction.[39] This result is in accordance with the SEM and EDX results.

XRD Pattern Analysis

The XRD analysis is used to calculate the inter planar (or) layer distance (d-spacing) between the polymer chains. Generally, the crystalline polymers show small d-spacing values than the amorphous polymers.[26] The d-spacing of the membrane decides its permeability and selectivity. Figure 8 illustrates the stacked XRD patterns of the bare and modified membranes. There is no significant increase in the d-spacing value for membrane a2 which is similar to the results obtained for the PI/TiO_2 mixed matrix membrane.[40] However, the nano MgO/SPPSU/PPSU membrane matrix showed decreases in intensity of the diffracted peak with the significant shift of 2θ angle. This decrease in intensity of the peaks confirms the increases in irregularity in the polymeric chain orientation of the membrane structure.[41] All the modified membranes (a3–a6) show significant increases in inter planar distance as given in Table II. This could be due to the formation of a loosely packed membrane structure. A maximum inter planar distance of 0.488 nm was observed for membrane a6. This could be due to (i) the nano MgO interacts with sulfonic acid groups of SPPSU polymeric chain reduces the strong interaction between sulfonic acid groups[42] (ii) an incompatibility in the interaction between bare PPSU and nano MgO-SPPSU polymeric chains.

Analysis of Porosity and Pore Size

The porosity, MWCO, and mean pore size of all prepared membranes are seen in Table II. The bare PPSU has a low porosity of 24.6% (±0.31). In the case of nano MgO decorated membranes, porosity values increased to 62.8% (±3.03) and 65.7% (±3.57) for membrane a5 and a6, respectively. In the case of membrane a2, addition of nano MgO did not significantly improve the pore size. This can be due to the more rigid structure that restricts the pore nuclei growth.[43] In the case of membranes (a3–a6), the hydrophilic nano MgO which migrated to the membrane surface forms a polymer–nanoparticles network and causes the stress at the interface.This could be due to repulsive forces between nano MgO-SPPSU and PPSU.[44] So, the formation of number surface pores is a quick relaxation to reduce the interfacial stress on the membrane surfaces.[45] In addition, all membranes show 40 kDa MWCO, except membrane a6. The SEM and XRD results also supported the porosity, MWCO, and mean pore size.

Flux, Rejection, and Fouling Resistance Analysis of Membranes against Humic Acid (HA) Solution

Figure 9 displays the HA solution flux profile of pure and modified membranes. The permeation properties mainly depend on the surface hydrophilicity and pore structure of the membrane. The modified membranes (a3–a6) show higher pure water permeation properties compared to membrane a1 and a2.

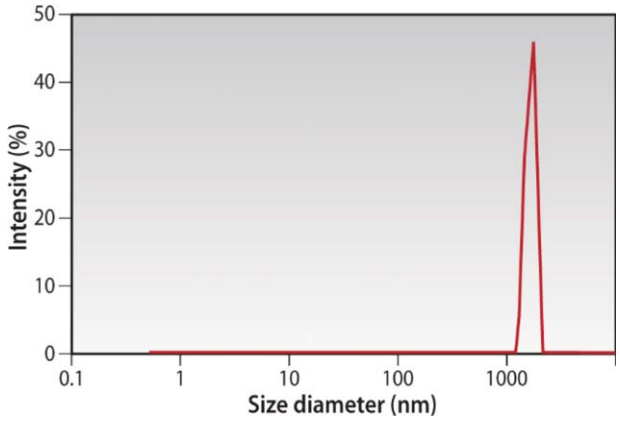

Figure 10. Dynamic light scattering (DLS) result of castor oil/water emulsion. [Color figure can be viewed in the online issue, which is available at wileyonlinelibrary.com.]

Table V. Flux, Rejection and Fouling Analysis of Membranes for Castor Oil/Water Emulsion (O/W)

Membrane	Flux ($Lm^{-2}h^{-1}$)			R_r (%)	R_{IR} (%)	FRR (%)	Rejection of O/W emulsion (%)
	J_{w1}	J_o	J_{w3} (SLS)				
a1	116 (±1.15)	37.8 (±1.7)	63.6 (±1.53)	22.3 (±0.49)	45.1 (±1.31)	54.8 (±0.1)	99 (±0.2)
a2	125 (±2.2)	45.4 (±1.1)	71 (±1.5)	20.5 (±0.23)	42.8 (±0.48)	57.2 (±0.5)	99 (±0.3)
a3	170 (±1.52)	57.4 (±0.57)	138.3 (±2.57)	47.5 (±2.4)	21.7 (±2.13)	81.2 (±0.1)	99 (±0.2)
a4	189 (±4.93)	69.4 (±0.4)	163.5 (±3.25)	49.7 (±1.43)	13.5 (±1.82)	86.4 (±0.2)	99 (±0.1)
a5	221 (±2.01)	79.6 (±1.0)	207.6 (±2.3)	57.9 (±1.73)	6.03 (±1.21)	93.8 (±0.1)	99 (±0.2)
a6	234 (±1.53)	83.5 (±0.8)	222 (±1.73)	59.1 (±0.99)	5.02 (±0.74)	94.9 (±0.3)	99 (±0.4)

This is due to the surface hydrophilicity and amorphous nature (larger segmental void volume) of modified membranes (a3–a6).[46] Here, the loss of nano MgO was assessed by an inductive coupled plasma mass spectroscopy (ICP-MS, Agilent model) for membranes (a3–a6). The concentration was below the detection limit.This is due to the strong acid–base interaction between the —SO_3H group and nano MgO, which could prevent the leachibility of nanoparticles from the membrane matrix. Further, these membranes were subjected to humic acid solution filtration. To the humic acid solution Ca^{2+} ions were added. These calcium ions form complexes with a carboxylic acid functional group of humic acid substances and increases the average size of the HA in the feed.[47] The pure PPSU membrane (a1) shows HA solution flux of 20 (±1.08) Lm^{-2} h^{-1}, which improved to 45 (±1.93) Lm^{-2} h^{-1} and 49.7 (±2.65) Lm^{-2} h^{-1} for hydrophilic membranes a5 and a6, respectively. Apart from a6 all membranes showed comparable rejection when challenged with HA as model foulant (Table III). The lower rejection of a6 can be explained on the fact that HA contains different range of molecular weight substance like humin, fluvic acid, and humic acid. Grasso *et al.*[48] mentioned the molecular weight of HA in the range of less than 10 kDa to more than 67 kDa. So, membrane a5 is observed to be an efficient membrane with high flux and required rejection.

It is seen that the hydrophilic membranes strongly reduce the irreversible fouling. So, the modified membranes (a3–a6) shows lower irreversible fouling (R_{ir}, %) values than the pure hydrophobic PPSU membrane a1 (see Table III). This result confirms that the presence of nano MgO on the membrane surface imparts fouling resistance to the membranes.

The resistance in a series model was used to quantify the different types of fouling of all membranes. Table IV showes the results of hydrodynamic resistance (R_m), pore plugging resistance (R_p), cake layer resistance (R_c), and total resistance (R_t). The pure PPSU membrane a1 shows a total resistance value of 6.94 (±0.36) which decreased to 3.04 (±0.50) for membrane a5 (see Table IV). The lower R_t of membrane indicates that nano MgO fixed membranes have poor pore plugging and cake layer resistance against foulants during filtration.[49]

Flux, Rejection, and Fouling Resistance Analysis of Membranes against Castor Oil/Water Emulsions

Figure 9 illustrates the flux profile for castor oil/water (O/W) emulsion. During filtration, accumulation oil on the layer near the membrane surface was suppressed by providing mechanical stirring at 500 rpm. However, membranes a1 and a2 experience severe flux decline during O/W emulsion filtration. However, the modified membranes (a3–a6) maintain a stable O/W flux profile (given in Table V). Figure 10 shows the size distribution curve of castor oil/water (O/W) emulsion as measured by a particle size analyzer. Recent literature[50] also reports that hydrophilic membrane surfaces repel the oil droplet and selectively removes the water from oil/water emulsion. Here, all modified membranes showed around 99% rejection (Table V). This is due to the larger size of emulsion droplets than the pore size of the membranes.

The antifouling property was analyzed for all membranes. Membranes a1 and a2 showed higher irreversible fouling than other membranes. However, the modified membranes (a3–a6) show significantly lower irreversible fouling. The previous literature[51] mentioned that the hydrophilic surfaces can behave as

Table VI. Results of Fouling Resistance in the Series Model of Membranes for Castor Oil/Water Emulsion (O/W)

Membrane	Membrane resistance $R_m \times 10^{11}$ (m^{-1})	Pore plugging resistance $R_p \times 10^{11}$ (m^{-1})	Cake layer resistance $R_c \times 10^{11}$ (m^{-1})	Total resistance $R_t \times 10^{11}$ (m^{-1})
a1	1.20 (±0.01)	0.98 (±0.05)	1.50 (±0.21)	3.69 (±0.16)
a2	1.12 (±0.01)	0.83 (±0.01)	1.09 (±0.01)	3.04 (±0.02)
a3	0.82 (±0.21)	0.18 (±0.03)	1.41 (±0.08)	2.42 (±0.09)
a4	0.73 (±0.15)	0.11 (±0.02)	1.15 (±0.03)	2.01 (±0.03)
a5	0.63 (±0.07)	0.04 (±0.02)	1.07 (±0.02)	1.74 (±0.02)
a6	0.59 (±0.09)	0.03 (±0.01)	1.04 (±0.01)	1.66 (±0.02)

oleophobic surfaces under water at the solid–water–oil interface. So, the irreversible fouling is significantly suppressed for modified membrane a6, the value (R_{ir}) is 5.02% (±0.74). Even adsorbed oil foulants are easily dislodged from the hydrophilic membrane surfaces (a3–a6). Recent literature reported that hydrophilic membranes have the higher free energy surface in the air and the hydration layer on the membrane surface lowers its surface free energy.[52] So, the resultant low surface free energy of membranes (a3–a6) prevents the further oil adsorption, effectively. The fabricated nano MgO anchored membrane shows a higher flux recovery (94.9% (±0.3) for oil/water emulsion compared with unanchored PPSU(a2) membranes (57.2 (±0.5). The significant improvement is the higher solution flux recovery of this membrane which is comparable and even higher as compared to other reported modified UF membranes.[1,2,53–55] The pore plugging resistance (R_p) of membranes is also significantly reduced (see Table VI). Therefore, the hydrophilic modified membranes (a3–a6) provide better permeation, rejection, and antifouling properties for O/W emulsion.

CONCLUSION

Based on the results of the present study, the following conclusions can be made:

The nano MgO anchored SPPSU/PPSU membranes were successfully prepared by the addition of various concentrations of SPPSU. The electrostatic attraction between SPPSU and nano MgO strongly immobilize the nano MgO on the PPSU membrane surface, which can be seen from EDX and SEM. The leachability results of nano MgO/SPPU/PPSU membranes confirmed their good compatibility behavior with nano MgO particles.

As seen in the earlier study using SPPSU/PPSU membranes[24] there is seen to be a great improvement in water permeability and hydrophilicity when nano MgO were incorporated into the SPPSU/PPSU membrane matrix. Importantly, it is understood that the anchored nano MgO hydrophilic particles showed tremendous improvement in the membrane properties, such as inter layer distance, hydrophilicity, flux, rejection, porosity, pore size, and oleophobicity against oil/water emulsion. This modification approach to be the best solution to control and minimize the membrane fouling. Therefore, nano MgO/SPPSU/PPSU membranes developed in this work may be used in various applications like wastewater treatment, bio molecule separation and catalytic membranes.

REFERENCES

1. Chen, W.; Peng, J.; Su, Y.; Zheng, L.; Wang, L.; Jiang, Z. *Sep. Purif. Technol.* **2009**, *66*, 591.
2. Zhu, X.; Tu, W.; Wee, K.-H.; Bai, R. *J. Membr. Sci.* **2014**, *466*, 36.
3. Luo, L.; Han, G.; Chung, T.-S.; Weber, M.; Staudt, C.; Maletzko, C. *J. Membr. Sci.* **2015**, *476*, 162.
4. Kong, J.; Li, K. *Sep. Purif. Technol.* **1999**, *16*, 83.
5. Ahmad, A. L.; Abdulkarim, A. A.; Oo, B. S.; Ismail, S. *Chem. Eng. J.* **2013**, *223*, 246.
6. Liu, Y.; Yue, X.; Zhang, S.; Ren, J.; Yang, L.; Wang, Q.; Wang, G. *Sep. Purif. Technol.* **2012**, *98*, 298.
7. Yuan, T.; Meng, J.; Hao, T.; Zhang, Y.; Xu, M. *J. Membr. Sci.* **2014**, *470*, 112.
8. Zinadini, S.; Zinatizadeh, A. A.; Rahimi, M.; Vatanpour, V.; Zangeneh, H.; Beygzadeh, M. *Desalination* **2014**, *349*, 145.
9. Yu, L.; Zhang, Y.; Zhang, B.; Liu, J.; Zhang, H.; Song, C. *J. Membr. Sci.* **2013**, *447*, 452.
10. Xiaochen, F.; Yanlei, S.; Xueting, Z.; Yafei, L.; Runnan, Z.; Jiaojiao, Z.; Zhongyi, J.; Junao, Z.; Yanyan, M.; Yuan, L. *J. Membr. Sci.* **2014**, *464*, 100.
11. Leo, C. P.; Cathie Lee, W. P.; Ahmad, A. L.; Mohammad, A. W. *Sep. Purif. Technol.* **2012**, *89*, 51.
12. Garcia-Ivars, J.; Alcaina-Miranda, M.-I.; Iborra-Clar, M.-I.; Mendoza-Roca, J.-A.; Pastor-Alcañiz, L. *Sep. Purif. Technol.* **2014**, *128*, 45.
13. Vatanpour, V.; Madaeni, S. S.; Moradian, R.; Zinadini, S.; Astinchap, B. *J. Membr. Sci.* **2011**, *375*, 284.
14. Zinadini, S.; Akbar, A.; Rahimi, M.; Vatanpour, V. *J. Membr. Sci.* **2014**, *453*, 292.
15. Akar, N.; Asar, B.; Dizge, N.; Koyuncu, I. *J. Membr. Sci.* **2013**, *437*, 216.
16. Li, J. H.; Shao, X. S.; Zhou, Q.; Li, M.-Z.; Zhang, Q.-Q. *Appl. Surf. Sci.* **2013**, *265*, 663.
17. Shukla, S. K. *Sens. Actuators B: Chem.* **2004**, *98*, 5.
18. Rao, Y.; Wang, W.; Tan, F.; Cai, Y.; Lu, J.; Qiao, X. *Appl. Surf. Sci.* **2013**, *284*, 726.
19. Han, W.; Yu, Y. J.; Li, N. T.; Wang, L. B. *Chin. Sci. Bull.* **2011**, *56*, 1216.
20. Rahimpour, A.; Jahanshahi, M.; Khalili, S.; Mollahosseini, A.; Zirepour, A.; Rajaeian, B. *Desalination* **2012**, *286*, 99.
21. Wang, J.; Bai, H.; Zhang, H.; Zhao, L.; Chen, H.; Li, Y. *Electrochim. Acta* **2015**, *152*, 443.
22. Yin, J.; Deng, B. *J. Membr. Sci.* **2014**, *479*, 256.
23. Venkatesha, T. G.; Nayaka, Y. A.; Chethana, B. K. *Appl. Surf. Sci.* **2013**, *276*, 620.
24. Thanigaivelan, A.; Kaleekkal, N. J.; Doraiswamy, M. *J. Appl. Polym. Sci.* **2015**, *132*, 41986.
25. Rajesh, S.; Maheswari, P.; Senthilkumar, S. *Chem. Eng. J.* **2011**, *171*, 33.
26. Jayalakshmi, A.; Rajesh, S.; Senthilkumar, S.; Mohan, D. *Sep. Purif. Technol.* **2012**, *90*, 120.
27. Kanagaraj, P.; Nagendran, A.; Rana, D.; Matsuura, T.; Neelakandan, S.; Karthikkumar, T.; Muthumeenal, A. *Appl. Surf. Sci.* **2015**, *329*, 165.
28. Liang, C. Y. A. *Sep. Purif. Technol.* **2012**, *92*, 57.
29. Li, Q.; Bi, Q.; Lin, H.; Bian, L.; Wang, X. *J. Membr. Sci.* **2013**, *427*, 155.
30. Hamzah, S.; Ali, N.; Mohammad, A. W.; Ariffin, M. M.; Ali, A. *J. Chem. Technol. Biotechnol.* **2012**, *87*, 1157.
31. Álvarez-blanco, S. *Desalination* **2015**, *360*, 87.
32. Saranya, R.; Kumar, M.; Tamilarasan, R.; Ismai, A. F.; Arthanareeswaran, G. *J. Chem. Technol. Biotechnol.* **2015**, DOI: 10.1002/jctb.4641.

33. Sathyamoorthy, K. M. R. *Indian Inst. Met.* **2012**, *65*, 49.
34. Zhao, S.; Yan, W.; Shi, M.; Wang, Z.; Wang, J. *J. Membr. Sci.* **2015**, *478*, 105.
35. Huang, J.; Wang, H.; Zhang, K. *Desalination* **2014**, *336*, 8.
36. Rabiee, H.; Hossein, M.; Abadi, D.; Vatanpour, V. *J. Membr. Sci.* **2014**, *472*, 185.
37. Ma, Y.; Shi, F.; Zhao, W.; Wu, M.; Zhang, J.; Ma, J.; Gao, C. *Desalination* **2012**, *303*, 39.
38. Huang, L.; Li, D.-Q.; Lin, Y.-J.; Wei, M.; Evans, D. G.; Duan, X. *J. Inorg. Biochem.* **2005**, *99*, 986.
39. Jayalakshmi, A.; Rajesh, S.; Mohan, D. *Appl. Surf. Sci.* **2012**, *258*, 9770.
40. Sun, H.; Ma, C.; Yuan, B.; Wang, T.; Xu, Y.; Xue, Q.; Li, P. *Sep. Purif. Technol.* **2014**, *122*, 367.
41. Rabiee, H.; Hossein, M.; Abadi, D.; Vatanpour, V. *Appl. Surf. Sci.* **2014**, *313*, 207.
42. Hyun, C.; Min, K. A.; Bum, H.; Taik, Y.; Ok, B.; Moo, Y. *J. Membr. Sci.* **2007**, *303*, 258.
43. Vatanpour, V.; Siavash, S.; Moradian, R.; Zinadini, S.; Astincha, B. *Sep. Purif. Technol.* **2012**, *90*, 69.
44. Rajabi, H.; Ghaemi, N.; Madaeni, S. S.; Daraei, P.; Ali, M.; Falsafi, M. *J. Membr. Sci.* **2014**, *332*, 60.
45. Sitter, K.; De. Dotremont, C.; Genné, I.; Stoops, L. *J. Membr. Sci.* **2014**, *471*, 168.
46. Tseng, H.-H.; Zhuang, G.-L.; Su, Y.-C. *Desalination* **2012**, *284*, 269.
47. Lin, T.; Lu, Z.; Chen, W. *Desalination* **2015**, *357*, 26.
48. Grasso, D.; Chin, Y.-P.; Weber, J. *Chemosphere* **1990**, *21*, 1181.
49. Bae, T.; Kim, I.; Tak, T. *J. Membr. Sci.* **2006**, *275*, 1.
50. Zhu, Y.; Xie, W.; Li, J.; Xing, T.; Jin, J. *J. Membr. Sci.* **2015**, *477*, 131.
51. Wang, B.; Liang, W.; Liu, W. *Chem. Soc. Rev.* **2014**, *44*, 336.
52. Zhang, P.; Tian, R.; Lv, R.; Na, B.; Liu, Q. *Chem. Eng. J.* **2015**, *269*, 180.
53. Ahmad, A. L.; Majid, M. A.; Ooi, B. S. *Desalination* **2011**, *268*, 266.
54. Wu, C.; Li, A.; Li, L.; Zhang, L.; Wang, H.; Qi, X.; Zhang, Q. *Desalination* **2008**, *225*, 312.
55. Gohari, R.; Halakoo, E.; Lau, W. J.; Kassim, M. A.; Matsuura, T.; Ismail, A. F. *RSC Adv.* **2014**, *4*, 17587.